IMPLEMENTATION OF A DECOUPLED CONTROLLER FOR A MAGNETIC SUSPENSION SYSTEM USING ELECTROMAGNETS MOUNTED IN A PLANAR ARRAY

D. E. Cox   N. J. Groom
NASA Langley Research Center
Hampton, VA

Abstract

An implementation of a decoupled, single-input/single-output control approach for the Large Angle Magnetic Suspension Test Fixture is described. Numerical and experimental results are presented. The experimental system is a laboratory model large gap magnetic suspension system which provides five degree-of-freedom control of a cylindrical suspended element. The suspended element contains a core composed of permanent magnet material and is levitated above five electromagnets mounted in a planar array.

1 INTRODUCTION

A research effort is underway at NASA Langley Research Center to demonstrate the magnetic suspension, positioning, and maneuvering of objects over wide ranges of attitudes. Future applications of this technology range from magnetic suspension of wind tunnel models to advanced spacecraft experiment isolation and pointing systems. As part of this effort, a Large Angle Magnetic Suspension Test Fixture (LAMSTF) has been designed and built. The LAMSTF is a small scale laboratory model of a Large Gap Magnetic Suspension System (LGMSS) which provides five degree-of-freedom control of a cylindrical suspended element that contains a core composed of permanent magnet material. The suspended element is levitated above five electromagnets mounted in a planar array. The LGMSS is a conceptual design of a ground based experiment which is to be used to investigate the technology issues associated with: magnetic suspension at large gaps, accurate suspended element control at large gaps, and accurate position sensing at large gaps [1]. The objectives of the LAMSTF effort were to investigate the feasibility of the LGMSS concept and to provide a test fixture for developing and demonstrating control approaches. A description of the LAMSTF and some of the control approaches which have been investigated are presented in [2]. LAMSTF suspended element parameters and the field components generated by the electromagnets at the centroid of the suspended element are given in the Appendix to this paper.

This paper presents the implementation of a single-input/single-output (SISO) control approach for the LAMSTF with numerical and experimental results. The control approach

which was implemented was developed in [3] using the extended linearized model developed in [4]. The control approach is proportional-derivative (PD), where the command torques and forces are functions of positions and derivatives of position. The design technique provides a dynamic compensator given the desired pole locations of the closed-loop system. Numerical results are obtained which compare the desired poles to the actual coupled pole locations for a candidate design. Experimental responses are also obtained on the LAMSTF testbed and compared to simulation results.

2 EQUATIONS OF MOTION

The equations of motion for the LAMSTF were developed in [4]. The LAMSTF configuration consists of five electromagnets mounted in a planar array. Figure 1 is a schematic representation of the LAMSTF configuration and defines the coordinate systems. The suspended element coordinate system consists of a set of orthogonal $\bar{x}, \bar{y}, \bar{z}$ body-fixed axes which define the motion of the suspended element with respect to inertial space. The suspended element coordinate system is initially aligned with an orthogonal x, y, z system fixed in inertial space. The open-loop equations of motion are determined by evaluating the forces
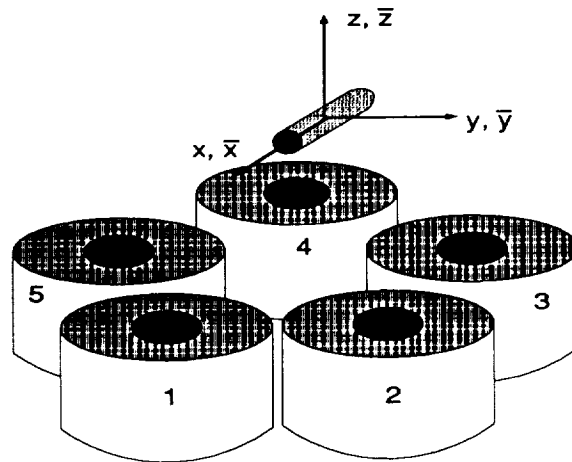
Figure 1: LAMSTF Configuration

and torques produced on the permanent magnet core by the magnetic fields [5]. They can be written as,

$$\dot{X} = f(X, I) \tag{1}$$

where

$$X = \begin{bmatrix} \Omega_{\bar{y}} & \Omega_{\bar{z}} & V_{\bar{x}} & V_{\bar{y}} & V_{\bar{z}} & \theta_y & \theta_z & x & y & z \end{bmatrix}^T$$

and

$$I = \begin{bmatrix} I_1 & I_2 & I_3 & I_4 & I_5 \end{bmatrix}^T$$

In the state vector, θ_y and θ_z are rotations about the y and z axis called pitch and yaw, respectively. The translations are x, y, and z, and Ω and V are time derivatives of the

corresponding positions. The input to the system are the five coil currents, denoted by I. In order to generate a linear model these equations are expanded about the nominal operating point X_o, I_o using a Taylor series expansion and simplified using small angle approximations. Higher order terms are neglected in the expansion and motion about the uncontrolled axis (x) is assumed to be zero. Details of the linearization are presented in [4]. The linearized equations have the form

$$\delta \dot{X} = \mathcal{A}\delta X + \mathcal{B}\delta I \tag{2}$$

where

$$\mathcal{A} = \left.\frac{\partial \dot{X}}{\partial X}\right|_{X_o, I_o} \quad \text{and} \quad \mathcal{B} = \left.\frac{\partial \dot{X}}{\partial I}\right|_{X_o, I_o}$$

Expanding these equations yields,

$$I_c \dot{\Omega}_{\bar{y}} = v M_{\bar{x}} \left(-B_x \theta_y - B_{xz} x - B_{yz} y - B_{zz} z\right) - v M_{\bar{x}} \mathbf{K}_z I \tag{3}$$

$$I_c \dot{\Omega}_{\bar{z}} = v M_{\bar{x}} \left(-B_x \theta_z + B_{xy} x + B_{yy} y + B_{yz} z\right) + v M_{\bar{x}} \mathbf{K}_y I \tag{4}$$

$$m_c \dot{V}_{\bar{x}} = v M_{\bar{x}} \left(-B_{xz} \theta_y + 2B_{xy} \theta_z + B_{xxx} x + B_{xxy} y + B_{xxz} z\right) + v M_{\bar{x}} \mathbf{K}_{xx} I \tag{5}$$

$$m_c \dot{V}_{\bar{y}} = v M_{\bar{x}} \left(B_{yz} \theta_y + (B_{yy} - B_{xx}) \theta_z + B_{xyx} x + B_{xyy} y + B_{xyz} z\right) + v M_{\bar{x}} \mathbf{K}_{xy} I \tag{6}$$

$$m_c \dot{V}_{\bar{z}} = v M_{\bar{x}} \left((B_{xx} - B_{zz}) \theta_y + B_{yz} \theta_z + B_{xzx} x + B_{xzy} y + B_{xzz} z\right) + v M_{\bar{x}} \mathbf{K}_{xz} I \tag{7}$$

where the B terms describe components and spatial derivatives of the magnetic field vector at the equilibrium point. The first subscript of B refers to a unit vector direction, while additional subscripts imply partial derivatives with respect to the coordinate system. The K coefficients are row vectors which define the fields produced by each coil per amp of current. I_c and m_c are inertia and mass of the core respectively, and $v M_{\bar{x}}$ is the product of the core's volume and magnetization. The first terms on the right in equations (3)-(7) are the torques and forces generated on the core due to perturbations in X, evaluated in the presence of the uncontrolled fields and gradients produced by the constant bias currents required to provide equilibrium suspension. The second terms are the torques and forces generated on the core by controlling the coil currents about the suspension currents. The controlled torques and forces can be written as,

$$\left[\begin{array}{c} \bar{T}_c \\ \bar{F}_c \end{array}\right] = \tilde{\mathcal{B}} I \tag{8}$$

where

$$\tilde{\mathcal{B}} = v M_{\bar{x}} \left[\begin{array}{c} -\mathbf{K}_z \\ \mathbf{K}_y \\ \mathbf{K}_{xx} \\ \mathbf{K}_{xy} \\ \mathbf{K}_{xz} \end{array}\right] \tag{9}$$

For the LAMSTF configuration $\tilde{\mathcal{B}}$ is full rank and the currents required to produce given

command torques and forces become

$$I = \tilde{B}^{-1} \begin{bmatrix} T_{\bar{y}c} \\ T_{\bar{z}c} \\ F_{\bar{x}c} \\ F_{\bar{y}c} \\ F_{\bar{z}c} \end{bmatrix} \tag{10}$$

For equilibrium suspension the torques and forces produced on the suspended element must be zero, except to counteract the effect of gravity. Therefore at equilibrium the suspension currents are

$$I_o = \tilde{B}^{-1} \begin{bmatrix} 0 \\ 0 \\ 0 \\ 0 \\ m_c g \end{bmatrix} \tag{11}$$

Although $\tilde{B}^{-1}$ decouples the five degrees of freedom in terms of force commands, the system dynamics are still highly coupled through the destabilizing bias terms in equations (3)-(7). The bias currents, I_o, are used to calculate the values of the bias fields and gradients presented in the Appendix. Many of these terms can be shown to be zero due to symmetry of the five-coil planar array. Referring to Figure 1, it can be seen that coil 1 is located symmetrically about the x, z plane and so cannot produce field components in this plane which are along the y axis. Furthermore, coils 2 and 5, and coils 3 and 4 form symmetric pairs about the x, z plane. These coil pairs have equal bias currents; therefore the projection along the y axis of fields from each pair is also zero throughout the x, z plane. This means that at X_o, the y component of the field is zero and all of its derivatives with respect to x and z are zero. Similar arguments can be used to show that B_{yy} and B_{zz} are also zero. Considering these zero terms, and making the additional approximation $B_{xxz} \simeq 0$ and $B_{xzx} \simeq 0$, equations (3)-(7) become,

$$I_c \dot{\Omega}_{\bar{y}} = -KB_x \theta_y - KB_{xz} x + T_{\bar{y}c} \tag{12}$$

$$I_c \dot{\Omega}_{\bar{z}} = -KB_x \theta_z + T_{\bar{z}c} \tag{13}$$

$$m_c \dot{V}_{\bar{x}} = KB_{xxx} x - KB_{xz} \theta_y + F_{\bar{x}c} \tag{14}$$

$$m_c \dot{V}_{\bar{y}} = KB_{xyy} y + F_{\bar{y}c} \tag{15}$$

$$m_c \dot{V}_{\bar{z}} = KB_{xzz} z + F_{\bar{z}c} \tag{16}$$

where the KB terms are constants equal to the product of $vM_{\bar{x}}$ and the corresponding field or gradient value evaluated at X_o, I_o. From these equations, it can be seen that the dynamics in y, z and θ_z are uncoupled and can be analyzed as single degree-of-freedom systems. The dynamics in θ_y and x, however, remain coupled. The strength of this interaction and its effect on SISO control design will be addressed in the next section.

The term KB_x in equations (12) and (13) is negative and causes open-loop instability. These terms cause high frequency unstable modes referred to as compass needle modes. Compass needle modes occur because, with the LAMSTF configuration, in order to achieve gradients which generate the vertical suspension force, the core's magnetization vector must

be aligned 180 degrees from the suspension field vector. These modes dominate the dynamics in pitch and yaw. The bias terms KB_{xxx} and KB_{xyy} also cause unstable dynamics. These terms are similar to the unstable bias flux stiffness terms encountered with small gap magnetic bearings that use permanent magnet bias flux [6, 7]. The terms KB_{xz} and KB_{xzz} cause stable coupling between x and θ_y, and stable oscillations in z. Eigenvalues for the LAMSTF open-loop system are presented in Table 1.

Mode	Eigenvalue	
Compass needle	-58.7793	
	58.7793	
Compass needle	-57.8061	
	57.8061	
y Translation	9.7764	
	-9.7764	
Stable Coupling	0.0000	+ 7.9697i
	0.0000	- 7.9697i
z Translation	0.0000	+ 0.9556i
	0.0000	- 0.9556i

Table 1: Eigenvalues of the open-loop system

3 CONTROL SYSTEM EQUATIONS

The control design technique allows the designer to directly place the poles of the closed loop system for each degree of freedom. Damping ratios and frequencies can be chosen to provide adequate response to disturbance inputs. The position of the suspended element is assumed to be known and is measured on the LAMSTF system by a set of five shadow sensors. As mentioned earlier, the control approach is PD, where the command torques and forces are functions of positions and derivatives of position. The command torques and forces can be written as

$$T_{\bar{y}c} = -\left(P_{\theta_y} + sR_{\theta_y}\right)\theta_y \qquad (17)$$

$$T_{\bar{z}c} = -\left(P_{\theta_z} + sR_{\theta_z}\right)\theta_z \qquad (18)$$

$$F_{\bar{x}c} = -\left(P_x + sR_x\right)x \qquad (19)$$

$$F_{\bar{y}c} = -\left(P_y + sR_y\right)y \qquad (20)$$

$$F_{\bar{z}c} = -\left(P_z + sR_z\right)z \qquad (21)$$

Position and rate gains are denoted P and R, respectively, for each degree of freedom. Control of pitch rotation and x translation will be examined first since these are the only suspended element motions which are coupled. The approach is to close the loop around each axis independently and to determine the effect of the cross-coupling on the performance of the resulting system. Equations (17) and (19) can be written in matrix form as

$$\left[\begin{array}{c} T_{\bar{y}c} \\ F_{\bar{x}c} \end{array} \right] = -G_F \left[\begin{array}{c} \theta_y \\ x \end{array} \right] \qquad (22)$$

where G_F is the forward-loop transfer function matrix,

$$G_F = \left[\begin{array}{cc} P_{\theta_y} + sR_{\theta_y} & 0 \\ 0 & P_x + sR_x \end{array} \right] \qquad (23)$$

Taking the Laplace transform of system equations (12) and (14) and putting them in matrix form results in

$$\left[\begin{array}{c} s^2 I_c \theta_y \\ s^2 m_c x \end{array} \right] = \left[\begin{array}{cc} -KB_x & -KB_{xz} \\ -KB_{xz} & KB_{xxx} \end{array} \right] \left[\begin{array}{c} \theta_y \\ x \end{array} \right] + \left[\begin{array}{c} T_{\bar{y}c} \\ F_{\bar{x}c} \end{array} \right] \qquad (24)$$

Substituting for $T_{\bar{y}c}$ and $F_{\bar{x}c}$ in (24) and collecting terms results in

$$\left[\begin{array}{cc} I_c s^2 + R_{\theta_y} s + P_{\theta_y} + KB_x & KB_{xz} \\ KB_{xz} & m_c s^2 + R_x s + P_x - KB_{xxx} \end{array} \right] \left[\begin{array}{c} \theta_y \\ x \end{array} \right] = 0 \qquad (25)$$

The characteristic equation becomes

$$\left| \begin{array}{cc} I_c s^2 + R_{\theta_y} s + P_{\theta_y} + KB_x & KB_{xz} \\ KB_{xz} & m_c s^2 + R_x s + P_x - KB_{xxx} \end{array} \right| = 0 \qquad (26)$$

Expanding the determinant yields

$$\left(s^2 + \frac{R_{\theta_y} s}{I_c} + \frac{P_{\theta_y} + KB_x}{I_c} \right) \left(s^2 + \frac{R_x s}{m_c} + \frac{P_x - KB_{xxx}}{m_c} \right) - \frac{(KB_{xz})^2}{I_c m_c} \qquad (27)$$

where the system's characteristic equation has been factored into two decoupled second order terms and a single coupling term. The coupling term in equation (27) is similar in form to the natural frequencies of the second order terms; however, it does not depend upon the feedback gains. It is possible to make this term negligible by increasing the position gains on the x and θ_y degrees of freedom. Ignoring the coupling term, the closed loop natural frequencies and damping for the θ_y mode can be written as

$$\omega_{\theta_y} = \sqrt{\frac{P_{\theta_y} + KB_x}{I_c}} \qquad \zeta_{\theta_y} = \frac{R_{\theta_y}}{2\sqrt{\left(P_{\theta_y} + KB_x \right) I_c}} \qquad (28)$$

Similarly for the x control loop

$$\omega_x = \sqrt{\frac{P_x - KB_{xxx}}{m_c}} \qquad \zeta_x = \frac{R_x}{2\sqrt{(P_x - KB_{xxx}) m_c}} \qquad (29)$$

Solving these equations for P and R yields design equations which allow for pole placement

$$P_{\theta_y} = \omega_{\theta_y}^2 I_c - KB_x \qquad R_{\theta_y} = 2\zeta_{\theta_y} \omega_{\theta_y} I_c \qquad (30)$$

$$P_x = \omega_x^2 m_c + KB_{xxx} \qquad R_x = 2\zeta_x \omega_x m_c \qquad (31)$$

The coupling term in equation (27) can only be ignored if the position gains are large, which implies that the SISO pole placement will be accurate only for sufficiently high frequencies. On the LAMSTF system this requirement was easily achieved. Table 2 shows design versus actual closed loop eigenvalues when the pitch and x loops are closed independently then analyzed as a coupled system. In each case the desired pole locations for the pitch and x modes were equal. Table 2 shows that the pole placement is inaccurate for low frequencies, but is reasonably accurate for frequencies above 75 rad/s, as expected. The table also shows very little variation between design and actual pole location for changes in damping.

SISO design poles		Coupled poles	
Frequency, rad/s	Damping	Frequency, rad/s	Damping
10.000	0.707	19.402	0.364
		22.117	1.000
30.000	0.707	34.299	0.618
		24.971	0.849
75.000	0.707	76.820	0.690
		73.133	0.725
100.000	0.707	101.372	0.697
		98.608	0.717
150.000	0.707	150.918	0.702
		149.075	0.711
75.000	0.100	76.820	0.097
		73.133	0.102
75.000	0.300	76.820	0.292
		73.133	0.307
75.000	0.500	76.820	0.488
		73.133	0.512
75.000	0.700	76.820	0.683
		73.133	0.717
75.000	0.900	76.820	0.878
		73.133	0.923

Table 2: Effect of coupling on accuracy of SISO pole placement

The characteristic equations for the remaining degrees of freedom can be obtained in a manner similar to the pitch and x loops. Since these loops are uncoupled, the design equations are exact. The compensator parameters as a function of damping ratios and natural frequencies are given by,

$$P_{\theta_z} = \omega_{\theta_z}^2 I_c - K B_x \qquad R_{\theta_z} = 2\zeta_{\theta_z}\omega_{\theta_z} I_c \qquad (32)$$

$$P_y = \omega_y^2 m_c + K B_{xyy} \qquad R_y = 2\zeta_y\omega_y m_c \qquad (33)$$

$$P_z = \omega_x^2 m_c + K B_{xzz} \qquad R_z = 2\zeta_z\omega_z m_c \qquad (34)$$

263

4 IMPLEMENTATION

The design method generates compensators which achieve approximate pole placement in the closed-loop system. The goal was to stabilize the experimental system and be able to maintain stability in the presence of disturbance forces. Poles were chosen to yield a system with a stiff response to disturbances and adequate damping to limit overshoot and oscillations.

As a design example the natural frequency of each closed-loop pole pair was set to 75 rad/s and the damping ratio of each was set to 0.707. Using equations (30)-(34) and parameters of the LAMSTF system, the position and rate gains were calculated. These gains are listed in Table 3. In the implementation of the PD controller it is desirable to

$$
\begin{array}{llll}
P_{\theta_y} & = 4.94 \times 10^{-2} & \text{Nm/rad} & R_{\theta_y} & = 5.84 \times 10^{-4} & \text{Nms/rad} \\
P_{\theta_z} & = 4.98 \times 10^{-2} & \text{Nm/rad} & R_{\theta_z} & = 5.84 \times 10^{-4} & \text{Nms/rad} \\
P_x & = 1.25 \times 10^{2} & \text{N/m} & R_x & = 2.35 & \text{Ns/m} \\
P_y & = 1.25 \times 10^{2} & \text{N/m} & R_y & = 2.35 & \text{Ns/m} \\
P_z & = 1.25 \times 10^{2} & \text{N/m} & R_z & = 2.35 & \text{Ns/m}
\end{array}
$$

Table 3: Position and rate gains for example design

limit the high frequency gain to minimize the effects of noise. Therefore, each PD loop was implemented as the following lead network,

$$
\frac{P_i + sR_i}{s/\omega_r + 1}
\tag{35}
$$

where the roll-off frequency, ω_r, is greater than the bandwidth of interest. In practice this was chosen to be 750 rad/second, an order of magnitude above the desired pole locations. A state-space model of the fully coupled system was developed and combined with the dynamic compensator to generate a continuous closed-loop system model. The damping ratios and natural frequencies of the poles of the closed-loop system are shown in Table 4. The frequencies are higher than designed due to the effects of the roll-off pole in the implementation.

The compensator designed above has been successfully implemented on the LAMSTF testbed. The suspended element position was derived from a set of five optical sensors arranged as shown in Figure 2. The sensors are based on power loss due to a shadowing of a collimated beam. The five measurements of the suspended element's position were sufficient to calculate the position and orientation in five degrees-of-freedom. The sensors are accurate to about 10 microns and have a linear range of about ± 1 mm. Dynamics from the sensor electronics are negligible.

An EISA-class 486 personal computer was used to implement the controller. Data acquisition, computation, and analog output were all handled by this computer. The controller was implemented as a set of discrete state space equations. The SISO continuous transfer functions were combined into a state space model and mapped into the discrete domain using a zero order hold transformation. The controller was implemented at a sample rate

264

Freq (rad/sec)	Damping
85.39	0.648
76.91	0.730
81.48	0.703
81.09	0.669
81.50	0.703
635.2	1.000
635.3	1.000
635.4	1.000
641.4	1.000
641.4	1.000

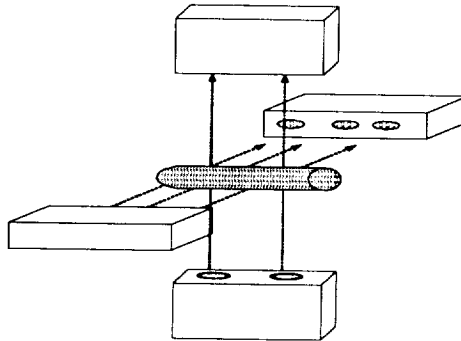Table 4: Natural frequencies and damping of closed-loop poles

Figure 2: Geometry of shadow sensor system

of 1 kHz. A computational delay of 0.43 msec separated the input sampling and analog output times. Performance of the controller was demonstrated by subjecting the suspended element to equivalent pulse disturbance forces. Actuator currents corresponding to a given disturbance force or torque are calculated for each degree of freedom using $\bar{B}$. These disturbances are implemented by adding these inputs to the closed-loop coil currents. Since the system has a nonzero steady-state error, the position of the suspended element tracks the input disturbance. Position of the element and the input torques and forces are plotted in Figure 3. The system remains stable and generally has a well damped response to the disturbances. Response in the yaw, x, y, and z degrees-of-freedom are all similar and consistent with design expectations. The response in pitch, however, contains slightly more overshoot and more oscillation than the other degrees-of-freedom. The cause of the underdamped response in pitch is currently being investigated and may be related to unmodeled dynamics from eddy current loops in the aluminum baseplate of the system. Additional testing and system identification are being performed to verify this hypothesis. A simula-
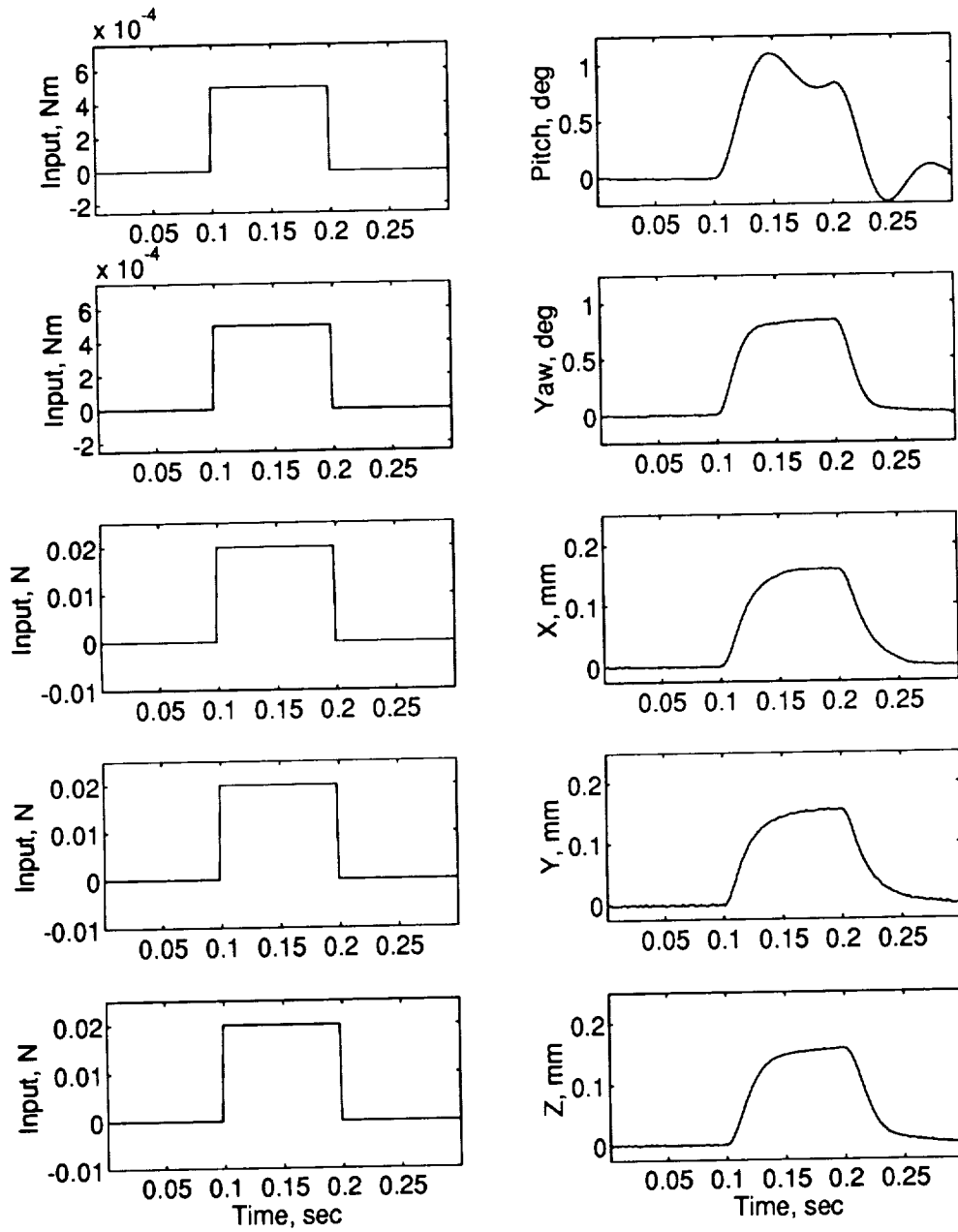
Figure 3: Experimental response to disturbance input

tion of the closed-loop system was developed with MATLAB's Simulink package [8]. The simulation models the continuous dynamics of the plant and considers the effect of sampling and computational delay in the implementation of the discrete controller. Figure 4 is a block diagram of the system as implemented in Simulink.
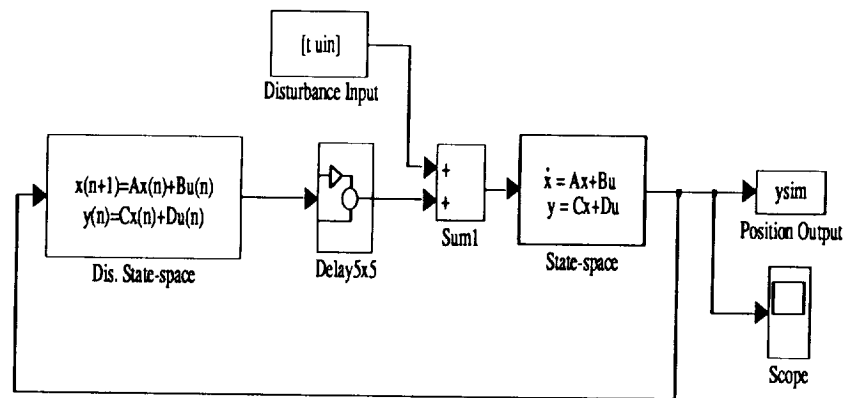

Figure 4: Block diagram of Simulink system simulation

Although the sampling frequency of 1 kHz is well above the closed loop dynamics, it was discovered that a pure analog analysis produced different responses than a simulation which considered the digital implementation. Figure 5 compares the full simulation, the experimental data, and an analog simulation. Response in pitch is underdamped experimentally, and the difference with respect to simulation can be easily seen. For the other degrees-of-freedom the digital simulation and actual response match quite well. The analog simulation, however, predicts a faster rise time and more overshoot in each case. A discrepancy between the frequency response of the continuous and discrete controllers was also noticed and appeared to be related to the high gain of the controller at the Nyquist frequency. Since the controller design was defined in the continuous domain, the differences between the digital and analog simulations are important to note.

5 CONCLUDING REMARKS

A decoupled control approach for a large gap magnetic suspension system has been presented. The magnetic suspension system is a planar array of electromagnets which provides levitation and five degree-of-freedom control of a cylindrical permanent magnet. The control approach assumes decoupled models for each degree of freedom. Position and rate gains for a dynamic compensator are computed based on desired pole locations. In the actual system, however, the system's dynamics remain coupled through bias terms resulting from the bias currents required to produce equilibrium suspension. The closed-loop performance, therefore, must be verified by applying the compensator to the coupled system model.

This technique provides the control designer simple and intuitive parameters to adjust in order to achieve closed-loop performance. In order to investigate the effects of coupling
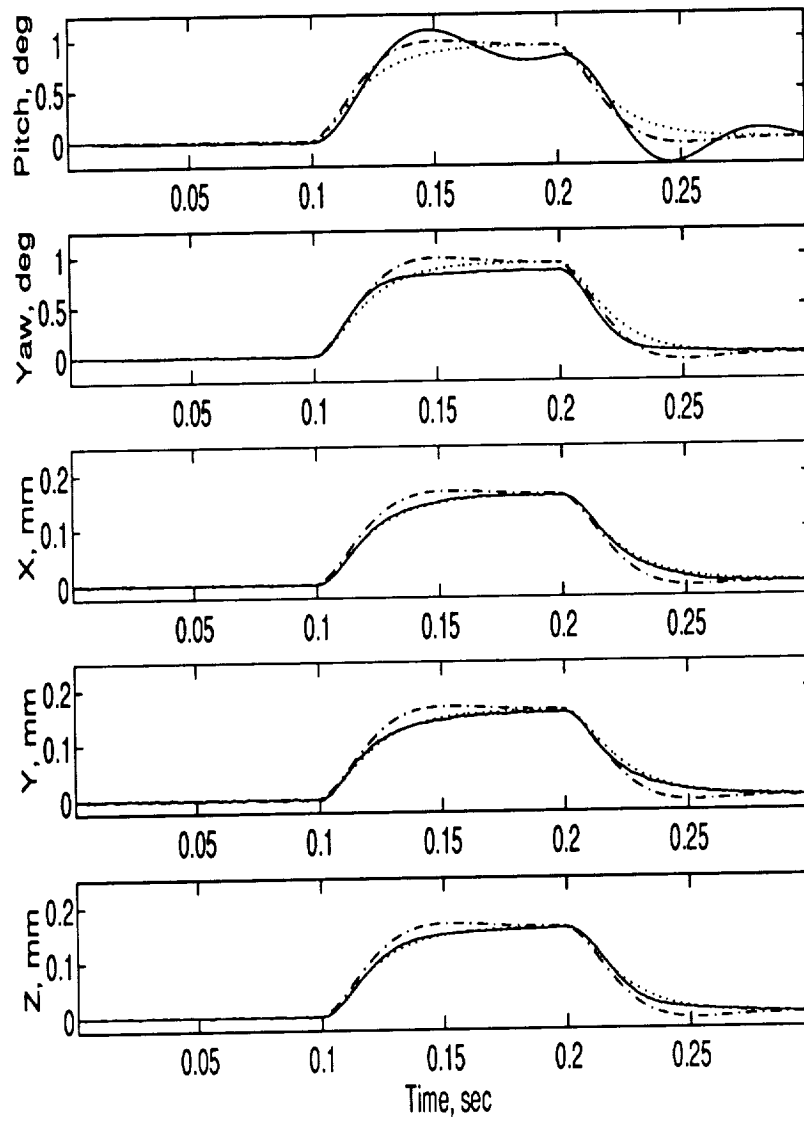
Figure 5: Comparison of experimental response (solid), digital simulation (dotted), and analog simulation (dash-dot)

between pitch and x translation, an example design was performed using the parameters of the Large Angle Magnetic Suspension Test Fixture (LAMSTF). Results of the design indicate that the damping ratios and natural frequencies of the coupled axes differ only slightly from design values. The control approach has been experimentally demonstrated on the LAMSTF system. Transient responses to pulse inputs compare favorably with simulations of the closed-loop system.

References

[1] Groom, N. J.: *Description of the Large Gap Magnetic Suspension System (LGMSS) Ground Based Experiment*. NASA CP-3109, Vol. 2, March 1991, pp. 365-377.

[2] Groom, N. J.; and Britcher, C. P.: *A Description of a Laboratory Model Magnetic Suspension Test Fixture with Large Angular Capability*. Proceedings of the First IEEE Conference on Control Applications, September 13-16, 1992, Dayton, Ohio, Vol. 1, pp.454-459.

[3] Groom, N. J.: *A Decoupled Control Approach for Magnetic Suspension Systems Using Electromagnets Mounted in a Planar Array*. NASA TM-109011, August 1993.

[4] Groom, N. J.; and Britcher, C. P.: *Open-Loop Characteristics of Magnetic Suspension Systems Using Electromagnets Mounted in a Planar Array*. NASA TP-3229, November 1992.

[5] Groom, N. J.: *Analytical Model of a Five Degree-of-Freedom Magnetic Suspension and Positioning System*. NASA TM-100671, July 1990.

[6] Groom, N. J.: *Analytical Model of an Annular Momentum Control Device (AMCD) Laboratory Test Model Magnetic Bearing Actuator*. NASA TM-80099, August 1979.

[7] Groom, N. J.; Woolley, C. T.; and Joshi, S. M.: *Analysis and Simulation of a Magnetic Bearing Suspension System for a Laboratory Model Annular Momentum Control Device*. NASA TP-1799, March 1981.

[8] Matlab 4.0 Users Manual, The Mathworks Inc. August 1992.

[9] The VF/GFUN Reference Manual, VF068894. Vector Fields Limited, June 1988.

A   APPENDIX

This appendix presents, in the form of tables, LAMSTF suspended element parameters, electromagnet parameters, and components of fields and gradients (including second-order gradients) generated by the LAMSTF electromagnets at the centroid of the suspended element. The LAMSTF contains a planar array of five room-temperature electromagnets, with iron cores, mounted in a circular configuration. The configuration is shown schematically in Figure 1. For a more detailed description of the LAMSTF see [2]. The fields and gradients were calculated using VF/GFUN [9], including the pre- and post-processor OPERA, with all iron cores modeled. Physical parameters of the LAMSTF are presented in table A1. Electromagnet fields and first-order gradients generated by the suspension currents at the equilibrium point are presented in table A2. The fields, first-order gradients and second-order gradients generated by each coil at the equilibrium point are presented in table A3. It should be noted that only non-zero terms are included and the full set of components is not listed in the tables since $B_{ij} = B_{ji}$ and $B_{ijk} = B_{ikj}$.

Core diameter	8.509×10^{-3} m
Core length	5.08×10^{-2} m
Suspended element mass, m_c	22.124×10^{-3} kg
Suspended element inertia, I_c	5.508×10^{-6}
Core volume, v	2.889×10^{-6} m^3
Core magnetization, $M_{\bar{x}}$	7.785×10^5 A/m
Suspension height	0.1 m
Electromagnet outer radius	0.0825 m
Electromagnet inner radius	0.0475 m
Electromagnet height	0.105 m
Iron core radius	0.038 m
Location radius*	0.1375 m

* Distance from center of array to axis of given coil

Table A1: Physical parameters of LAMSTF

Component	Field strength, Tesla
B_x	-8.1863e-03
B_{xz}	9.6504e-02
B_{xxx}	4.9139e-01
B_{xxz}	-2.4689e-04
B_{xyy}	9.4051e-01
B_{xzz}	-8.9865e-03

Table A2: Values of bias fields and gradients at suspension point

270

Component	Fields, Tesla/Amp				
	Coil 1	Coil 2	Coil 3	Coil 4	Coil 5
K_x	2.3100e-04	7.1000e-05	-1.8700e-04	-1.8700e-04	7.1000e-05
K_y	0	2.2000e-04	1.3600e-04	-1.3600e-04	-2.2000e-04
K_z	-9.4000e-05	-9.4000e-05	-9.4000e-05	-9.4000e-05	-9.4000e-05
Component	First-order field gradients, Tesla/m/Amp				
	Coil 1	Coil 2	Coil 3	Coil 4	Coil 5
K_{xx}	2.1790e-03	-1.5030e-03	7.7200e-04	7.7200e-04	-1.5030e-03
K_{xy}	0	1.1960e-03	-1.9360e-03	1.9360e-03	-1.1960e-03
K_{xz}	-2.7230e-03	-8.4100e-04	2.2030e-03	2.2030e-03	-8.4100e-04
K_{yy}	-1.8920e-03	1.7900e-03	-4.8500e-04	-4.8500e-04	1.7900e-03
K_{yz}	0	-2.5900e-03	-1.6000e-03	1.6000e-03	2.5900e-03
K_{zz}	-2.8700e-04	-2.8700e-04	-2.8700e-04	-2.8700e-04	-2.8700e-04
Component	Second-order field gradients, Tesla/m^2/Amp				
	Coil 1	Coil 2	Coil 3	Coil 4	Coil 5
K_{xxx}	3.4340e-03	-1.8276e-02	1.6559e-02	1.6559e-02	-1.8276e-02
K_{xyx}	0	-1.4560e-02	1.3733e-02	-1.3733e-02	1.4560e-02
K_{xzx}	-5.3466e-02	1.6371e-02	-2.6790e-02	-2.6790e-02	1.6371e-02
K_{xyy}	-2.1916e-02	-1.1938e-02	2.2896e-02	2.2896e-02	-1.1938e-02
K_{xyz}	0	8.7350e-03	-1.4134e-02	1.4134e-02	-8.7350e-03
K_{xzz}	2.5400e-04	7.8000e-05	-2.0500e-04	-2.0500e-04	7.8000e-05

Table A3: Field and gradient values for each coil, Tesla/Amp

Session 6b – MSBS

Chairman: Colin P. Britcher
Old Dominion University